Title	A model of hoarfrost formation on a cable
Author(s)	Lasse Makkonen
Citation	Cold Regions Science and Technology. Vol. 85 (2013) No: January, pages 256 - 260
Date	2013
URL	http://dx.doi.org/10.1016/j.coldregions.2012.10.001
Rights	This article may be downloaded for personal use only.

REVISION 3

A model of hoarfrost formation on a cable

Lasse Makkonen[1]

VTT Technical Research Centre of Finland, Box 1000, 02044 VTT, Espoo, Finland

Abstract

A time-dependent numerical model of hoarfrost formation on an overhead cable is presented. The model is aimed at calculating the thickness of a hoarfrost layer using routinely measured meteorological data as input. The growth rate and density of hoarfrost are simulated. This requires continuous calculation of the surface temperature around the cable. The model also simulates the disappearance of hoarfrost by sublimation, melting and dropping off. The feasibility of explaining the occurrence of corona losses on overhead power transmission cables by the modelled hoarfrost thickness is demonstrated by field data.

Keywords: hoarfrost; frost; icing; ice accretion; ice growth; power line; corona loss

---

[1] Tel.: +358 20 722 4914; fax: +358 20 722 7007
E-mail address: lasse.makkonen@vtt.fi

Nomenclature

C	corona loss in electric power transmission, MW
c_c	specific heat of the cable material, J/(kg K)
c_p	specific heat of air, J/(kg K)
d	cable diameter, m
D	iced cylinder diameter, m
e_a	water vapor pressures in air, Pa
e_s	water vapor pressure over ice, Pa
g	gravitational constant, m/s^2
Gr	Grashof number
H	mean thickness of the simulated hoarfrost deposit, mm
h	convective transfer coefficient, $h = k_a Nu/D$, W/(m^2 K)
I	rate of ice formation, kg/(m^2 s)
k_a	heat conductivity of air, W/(m °C)
k_i	heat conductivity of the simulated hoarfrost deposit, W/(m K)
L_e	latent heat of sublimation of ice at t_s, J/Kg
n	cloudiness, parts of ten
Nu	Nusselt number

Nu_v	Nusselt number in free convection
Nu_b	Nusselt number in forced convection
p_a	atmospheric pressure, Pa
q_c	flux of sensible heat to air, W/m^2
q_e	heat flux due to release of latent heat of sublimation, W/m^2
q_{eff}	effective outgoing long wave radiation flux, W/m^2
$q_{eff,0}$	outgoing long wave radiation flux at clear skies, W/m^2
q_i	conductive heat flux onto the ice surface through ice, W/m^2
q_S	effective Sun’s short wave radiation flux, W/m^2
Q_J	Power due to Joule heating of the cable, W/m
Q_t	Power due to thermal inertia of the cable, W/m
Re	Reynolds number, vD/υ
t_a	air temperature, °C
T_a	air temperature, K
t_c	cable temperature, °C
T_c	cable temperature, K
t_s	ice surface temperature, °C
T_s	ice surface temperature, K

v	wind speed, m/s

Greek symbols

υ	cinematic viscosity of air, m^2/s
σ	Stefan-Bolzmann coefficient, $J/(m^2K^4)$
ρ	density of the forming hoarfrost, kg/m^3
ρ_c	density of the cable material, kg/m^3
ρ_t	simulated overall hoarfrost density, kg/m^3
ΔT_c	decrease in cable temperature during a model time-step, K
$\Delta\tau$	time-step in the model, s

1. Introduction

Hoarfrost forms when water vapour changes directly into solid ice. Under natural atmospheric conditions the resulting ice deposition consists of loosely spaced needle-like thin ice crystals (Figure 1). The dimensions of hoarfrost deposits are usually small and the density of them is very low. Hoarfrost is easily blown off by the wind. Consequently, hoarfrost alone does not cause ice loads or aerodynamic effects that are significant to structural safety, unlike rime, glaze and wet snow (Makkonen, 2000).

Figure 1. Hoarfrost on a crabapple showing the typical needle-like microstructure and nonsymmetrical accretion. Photo by S. von Schroeder.

Nevertheless, hoarfrost causes problems, particularly on overhead cables on which it is related to corona discharges and consequent power losses (Lahti et al. 1997). Corona losses in power transmission are caused also by precipitation, but their magnitude is at its greatest when the electric field at the conductor surface is enhanced by the presence of the ice needles of a hoarfrost deposition. This phenomenon causes electricity transmission losses that are of significant economic value in cold regions (Sollerkvist et al., 2007). Furthermore, on overhead cables for trains and trolleys, hoarfrost causes a corona discharge at the contact with the pantograph, causing excess wear and a light and noise problem (Kamata et al., 2012).

During hoarfrost formation in nature the humidity of air is not necessarily high. The outgoing long wave radiation may cool the surface so much that deposition occurs even at a relatively low humidity. When the air is so humid that it is saturated with respect to ice, deposition occurs even without the radiation cooling effect. Thus, hoarfrost may form simultaneously with in-cloud icing. Intensive icing due to accreting droplets may then occur and the portion of the icing rate due to vapour deposition is typically small. However, the rate of hoarfrost formation is approximately proportional to the surface area, whereas the rate of rime icing increases more slowly with increasing object size. Therefore, for ice load modelling on very large objects hoarfrost may need to be taken into account. Moreover, very accurate modelling of rime icing, required by the rotating multi-cylinder method to measure cloud liquid water and droplet size, must include vapour deposition (Makkonen, 1992).

Hence, there are several applications in which numerical modeling of hoarfrost formation under natural conditions is useful. The best prospect in utilizing hoarfrost modeling is in the significant savings to be achieved if hoarfrost on cables could be predicted using a weather forecasting model and reduced by controlled Joule heating. Here, a physical-numerical model of hoarfrost is proposed. In contrast to some other models of frost formation on planar surfaces and in industrial applications (Schneider, 1977; Hayashi et al., 1977; Saito et al., 1984; Seki et al., 1984; Östin and Andersson, 1991; Raju and Sherif, 1992; Mago and Sherif, 2005; Kandula, 2011), this model is developed specifically for simulating hoarfrost thickness on a cable in a natural outdoors environment.

2. The model

The foundation of this hoarfrost formation model is the cylinder icing model by Makkonen (1984), discussed also in Poots (1996) and Makkonen (2000). The changes made to the icing model for this study on hoarfrost are:

1. A sub-program simulating vapor depostion rate and hoarfrost density is included, as will be explained below.
2. Free convection is taken into account in the heat balance because hoarfrost may form when there is no wind.
3. The outgoing long wave radiation and Sun's direct radiation are included in the heat balance since hoarfrost may form during clear skies.
4. The heat balance is calculated separately on the windward side and the lee side, and on the upper side and lower side of the object.
5. Heat transfer from the conductor to the surface of ice is modeled. This allows including the effects of the Joule heating and cable thermal inertia.
6. The heat balance terms related to droplet impingement are neglected since this model is for simulating hoarfrost only. A necessary input then is the humidity of air.
7. Ice disappearance is modeled by including evaporation and melting, as well as a criterion of ice release by shedding. This makes long-term continuous modeling possible.

The model simulates the mean rate of ice accretion, i.e. the deposition rate, and the mean thickness of the accretion around the cable. They are based on modeling icing at four sections around a horizontally oriented cable. This requires solving numerically the heat balance and surface temperature of these sections, as discussed in the following.

2.1 Deposition

The vapor deposition rate is I calculated by eq. (1). When I is negative, sublimation of ice occurs (when the simulation shows ice on the section surface).

$$I = \frac{0.62}{c_p p_a} h\left(e_s - e_a\right) \tag{1}$$

Here c_p is the specific heat of air, p_a the atmospheric pressure, h the convective transfer coefficient and e_s and e_a the water vapor pressures over ice and in air, respectively. The convective transfer coefficient h depends mainly on wind speed and cable diameter as well as surface roughness, see below and Makkonen (1985). The vapor water pressure in air, e_a, is an input parameter for the modeling. It is typically obtained by measuring the relative humidity and temperature in air. The equilibrium water vapor pressure over ice, e_s, depends on the surface temperature of the ice, t_s, the modeling of which is, therefore, a critical issue here. Moreover, eq. (1) only applies when $t_s < 0$ °C.

2.2 The heat balance

The surface temperature of the ice, T_s, is solved from the heat balance of the section of the cable by numerical iteration.

With the assumptions explained above the heat balance in the model is

$$q_e + q_s + q_i = q_c + q_{eff} \tag{2}$$

where the heat flux terms are explained in the nomenclature and discussed in the following.

2.2.1 Convective heat transfer

The heat flux due to release of latent heat of phase change from vapor to ice is

$$q_e = L_e\, I \tag{3}$$

where L_e is the latent heat of sublimation of ice at t_s.

The heat flux due to convective heat transfer to air is

$$q_c = h\left(T_s - T_a\right) \tag{4}$$

Both q_e and q_c depend on the convective heat transfer coefficient

$$h = k_a\, Nu/D \tag{5}$$

which is calculated separately on the upper side and lower side of the cable, and in the presence of wind separately on the windward and the leeward surfaces. Here k_a is the heat conductivity of air, D is the iced cylinder diameter and Nu is the Nusselt number.

In free convection the Nusselt number is calculated by Sparrow and Stretton (1985)

$$Nu_v = 0.395\, Gr^{0.25} \tag{6}$$

where Gr is the Grashof number

$$Gr = \frac{gD^3\left|T_s - T_a\right|}{\upsilon^2 T_a} \tag{7}$$

Here g is the gravitational constant, υ is the kinematic viscosity of air, T_s the ice surface temperature and T_a the air temperature. Free convection, calculated by eq. (6), is assumed to affect the upper side of the cable when $T_s < T_a$ (downward flow) and the lower side of it when $T_s > T_a$ (upward flow).

In forced convection, at a wind speed *v*, the Nusselt number is calculated by the Reynolds number $Re = vD/\upsilon$ as

$$Nu_b = a\mathrm{Re}^{0.85} \tag{8}$$

In eq. (8) the constant *a* is 0.032 for the windward side and 0.007 for the lee side. This equation gives allowance to the roughness of the ice surface (Makkonen, 1984). In the simulations the bigger of Nu_v and Nu_b is applied for each section of the iced cable surface separately.

2.2.2 Radiation heat transfer

Because hoarfrost forms also at clear skies, a treatment of radiation in the heat balance is necessary. In fact, the outgoing long-wave radiation is the main driving force for hoarfrost formation as it cools the surface and thus lowers e_s in eq. (1).

The outgoing long wave radiation flux is calculated by eq. (9)

$$q_{eff,0} = T_s^4 - T_a^4\left(0.58 + 0.044\sqrt{e_a}\right) \tag{9}$$

where σ is the Stefan-Bolzmann coefficient. Equation (9) is applied on the upper section of the cable only, which includes the assumption that the radiation fluxes from the ground and from the lower side of the cable cancel out. In other words, the iced cable emits long-wave radiation into the half-space above. A correction for cloudiness is made by

$$q_{eff} = (1 - 0.08n)\ q_{eff,0} \tag{10}$$

where n is cloudiness in parts of ten. These and other long-wave radiation flux parameterizations from ice and snow surfaces are discussed in detail in e.g. Gray and Male (1981) and Sedlar and Hock (2009).

Short-wave radiation by the Sun, q_S, is typically a small term here, because the formation of hoarfrost usually occurs during dark hours. Moreover, the reflection coefficient for short-wave radiation from a hoarfrost surface is similar to that of fresh snow, i.e. more than 90% (Gray and Male, 1981, p. 34) and that from a non-iced aluminum cable is similar. However, q_S can be included in the modeling when the data are available from measurements at weather stations. Moreover, when direct radiation measurements are unavailable, q_S may be parameterized based on the latitude, time of year, time of day and corrections based on the cloudiness and humidity of air (Gray and Male, 1981).

2.2.3 Conductive heat transfer

The conductive heat flux to the surface of the hoarfrost layer q_i equals the heating power originating from the cable divided by the surface area. An electric cable emits heat in stationary conditions as the Joule heating Q_J. Additionally, in varying conditions, the thermal inertia of the cable may produce a heating/cooling power, Q_t. Thus,

$$q_i = (Q_J + Q_t)/(\pi D) \tag{11}$$

In the modeling, the Joule heating, Q_J, is given as input based on the known cable electric resistance and the instantaneous current.

The instantaneous power by the thermal inertia, Q_t, in eq. (11) is calculated based on the changes in the atmospheric conditions and the electric current within a time-step of the model. This requires simulation of the temperature of the cable, which is calculated based on the cylindrical geometry as

$$T_c = T_s + D\ln\left(D/d\right)q_i/\left(2k_i\right) \tag{12}$$

where d is the cable diameter and k_i is the heat conductivity of the hoarfrost estimated by

$$k_i = 0.0242 + 0.0002\rho_t + 2.54\cdot 10^{-6}\cdot\rho_t^2 \tag{13}$$

Here, ρ_t is the simulated overall hoarfrost density (see 2.4). Equation (13) is a modified extension of an empirical equation by Yonko and Sepsy (1967). The power per unit length of the cable caused by thermal inertia within a time-step $\Delta\tau$ of the model is then calculated as

$$Q_t = \pi\left(d/2\right)^2 \rho_c c_c\,\Delta T_c/\Delta\tau \tag{14}$$

where ρ_c and c_c are the density and the specific heat of the cable material respectively and ΔT_c is the calculated decrease in the cable temperature during a time step of $\Delta\tau$.

2.4 Hoarfrost density

The density of the forming hoarfrost, ρ, is calculated based on the surface temperature, t_s, of that side of the cylinder where the rate of ice formation, I, is the highest. This is justified by test runs showing that the accretion is typically quite unsymmetrical with insignificant icing on the other sections. The hoarfrost density is calculated by eq. (15) presented in Hayashi et al. (1977). This equation is based on experimental data in the range -25 °C < t_s < 0 °C and 2 m/s < v < 6 m/s.

$$\rho = 650\, e^{0.227 t_s} \tag{15}$$

The density of the overall accretion ρ_t and the thickness of the ice layer are calculated cumulatively after each time-step as explained in Makkonen (1984). When there is disappearance of ice, the density of the lost ice is taken to be that of the overall density.

3. Running the model

The model calculates the heat balance and the rate of hoarfrost formation separately on the windward side and the lee side and on the upper side and lower side of the object. The output of the model is the mean thickness of the simulated hoarfrost around the cable, H. Disappearance of hoarfrost by sublimation occurs in the model when eq. (1) gives negative values and ice exists on the cable. In addition, when the modeled cable temperature, t_c (see eq. (12), reaches 0 °C, all ice is assumed to shed or melt. No icing is modeled as long as $t_c \geq$ 0 °C. Shedding of the hoarfrost deposit due to wind or cable dynamics alone is not considered.

The model is programmed in Visual Basic. The input for simulations can be given manually or be read directly from meteorological observation data files. In the latter case, the output is given by the model at intervals which correspond to the input. This is three hours for synoptic meteorological data. However, the internal calculation time-step of the model is much shorter for better accuracy. It is 10 seconds for the first 10 minutes of icing and 360 seconds after that. Test with the model showed that time-steps shorter than this do not change the output within the desired resolution.

The simulation of hoarfrost formation on a power line cable by the model requires as input

- Cable diameter
- Cable specific heat capacity
- Joule heating by the cable (when existent)
- Wind speed
- Air temperature
- Humidity in air
- Cloudiness
- Sun's radiation (when significant)

4. Results and discussion

Test runs using weather data in Finland showed that the model typically predicts a hoarfrost thickness of 0–15 mm, which corresponds to observations in nature. The results show systematic variations according to the time of day, as one would expect (Figure 2). The modeled hoarfrost cover typically forms in the night and disappears during the day.

In order to evaluate the sensitivity of the model to the meteorological parameters, it was run by changing one input variable at a time keeping the other input conditions fixed. The relationships revealed correspond well to what is qualitatively observed (Kamata et al, 2012) and, while complex, provide a deeper understanding of hoarfrost formation. The results of the model for the hoarfrost thickness H are quite sensitive to cloudiness, for example. This is shown as in Figure 3. Wind induced convection tends to prevent the ice surface temperature from falling well below that of air, thus resulting in a hoarfrost deposit with a lower density. Therefore, *H* increases with decreasing wind speed as shown in Fig. 3.

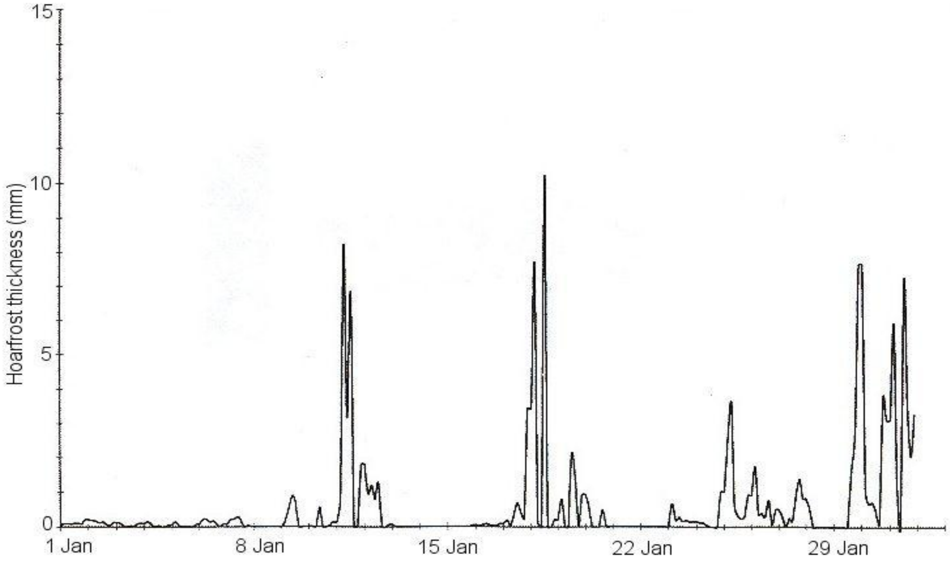

Figure 2. Example of a model output for hoarfrost thickness on a power line cable when using synoptic weather data (Kajaani, Finland, January 1994).

The dependence of the modeled hoarfrost thickness *H* on the relative humidity in air is shown in Fig. 4. This relationship is similar to that of the mass of sublimated ice. In contrast, a thicker hoarfrost layer at a colder temperature, also shown in Fig. 4, is entirely due to the effect of temperature on the density of the hoarfrost, as the modeled ice mass increases with increasing air temperature at a fixed relative humidity.

The model results critically depend on the input for the humidity in air as shown in Figure 4. In nature, vapor deposition often occurs in air that is supersaturated with respect to ice. The degree of super-saturation then controls the growth rate of hoarfrost. However, the degree of supersaturation is not revealed at all by routine measured weather station data. This is because when hoarfrost forms, ice deposits on the humidity probes as well (Makkonen and Laakso, 2005). Consequently, the conventional humidity probes show a humidity reading that is locked at the saturation value with respect to ice, even when the true value is well above it (Makkonen and Laakso, 2005). This fundamental problem in the measurements removes, from the data, all real variation in the air humidity under supersaturated conditions. It thus seriously hampers detecting the correlation between the modeled and real hoarfrost thickness.

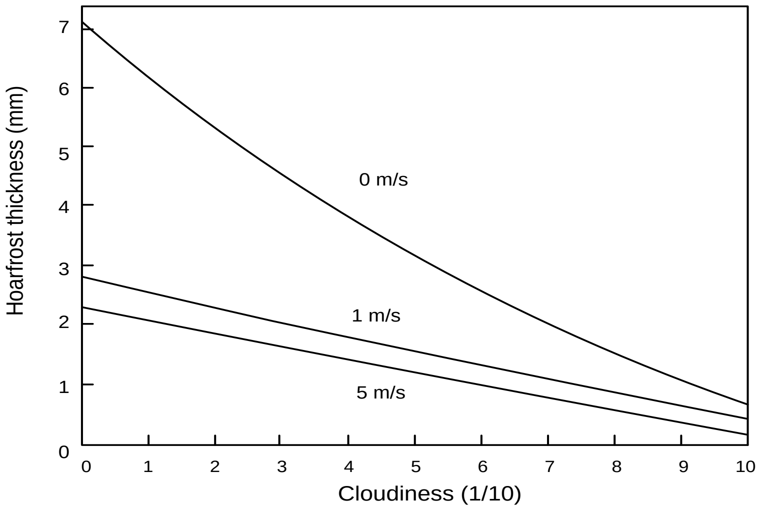

Figure 3. Modeled hoarfrost thickness vs. cloudiness at three wind speeds in a 10-hour simulation on a 50 mm diameter cable at air temperature of -10 °C and relative humidity of 90%.

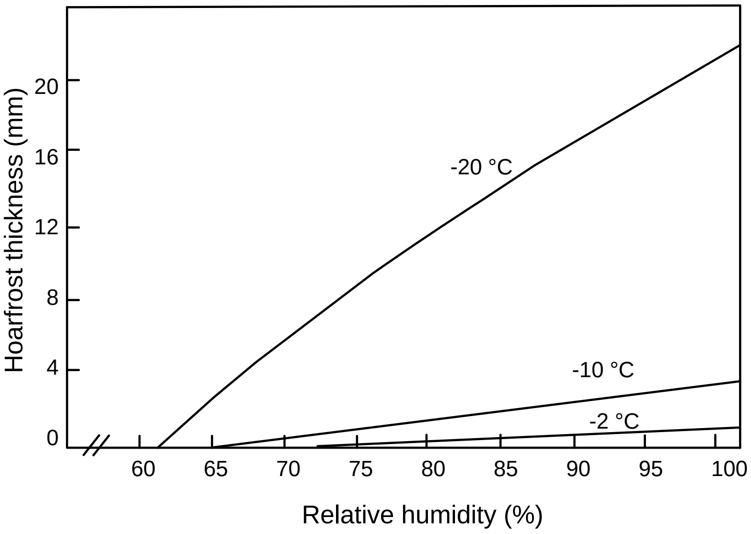

Figure 4. Modeled hoarfrost thickness vs. relative humidity at three air temperatures in a 10-hour simulation on a 50 mm diameter cable at a wind speed of 1 m/s and clear sky.

In future applications, humidity measurements made by a special sensor that provides correct values also at supersaturated conditions should be utilized (Makkonen and Laakso, 2005). Until then, it is not possible to fully verify the hoarfrost model quantitatively by direct observations of hoarfrost thickness in the field. Unfortunately, the model cannot be tested in a laboratory either, because the main driving force of hoarfrost formation, the effective outgoing long-wave radiation, is non-existent indoors. However, it is possible to test the model in its most important application directly, as discussed in the following.

The feasibility of the model in detecting the corona loss in power transmission was tested in large scale. Data for the corona loss in the 360 km long 400kV overhead power line Alapitkä–Petäjäkoski in central Finland were used for the purpose. These power loss data were measured by a power utility IVO Voimansiirto Oy by a method discussed by Sollerkvist et al. (2007). The input for the hoarfrost model was obtained from four weather stations operated by the Finnish Meteorological Institute along the route of the power line.

The comparison between the modeled hoarfrost and the measured corona loss was made for the period 1^{st} January–30thApril 1994. Hoarfrost thickness was modeled at three-hour intervals for this period at each weather station. A weighted average of these values was considered to represent the entire line. The weights given for each weather station were based on their geographical representativeness along the line.

The results show a significant correlation between the modeled occurrence of hoarfrost and the measured corona loss C, particularly when the events with precipitation are removed from the data. This relationship is shown in Table 1 where $C \leq 0.5$ means "insignificant loss" $0.5 < C < 2$ "moderate loss" and $C \geq 2$ "significant loss" as classified by the power utility. Table 1 shows, for example, that out of the cases where the model shows no hoarfrost, only 3% show moderate or significant corona loss. When the model shows more than 2 mm hoarfrost thickness the corona loss is moderate or significant in 82% of the cases. The hoarfrost model, thus, predicts the occurrence of a corona loss in large scale quite well and is definitely a useful tool in detecting the conditions prone to corona losses.

Table 1. Modeled mean hoarfrost thickness H (mm) and measured corona loss C (MW) on the 360 km long overhead power line. The observations are at three-hour intervals over a period of four months. Cases when a weather station reports precipitation are excluded.

	$H = 0$	$0 < H < 2$	$H \geq 2$
$C \leq 0.5$	186	77	15
$0.5 < C < 2$	5	67	24
$C \geq 2$	1	40	45

However, there is only a weak correlation (*r* = 0.47) between the modeled thickness of the hoarfrost accretion and the measured quantitative corona loss in these data of 460 observations. This is not surprising considering the fundamental problem in the input for air humidity, discussed above. Another problem with the input data is that unobserved local phenomena, such as snow showers and high humidity at river crossings, may have occurred along the power line route between the weather stations.

On the other hand, there may also be weaknesses in the model. For example, the possibility that the electric field on the cable affects the hoarfrost formation (Teisseyre and Farzaned, 1990) is not taken into account, because it has been considered unlikely that such an effect would cause a feedback between the corona discharge and ice amount (Zhang et al., 2006). Modeling the hoarfrost thickness as the mean over the cable circumference may not be ideal in this application and options for that will be studied in the future.

A particularly interesting result of the modeling is that the sensitivity tests for the entire 360 km long power line showed a significant reduction in the frequency of hoarfrost by a rather small increase in the Joule heating. This may provide means to control the hoarfrost formation on power lines in order to reduce corona losses. Another interesting prospect is the short-term forecasting of corona losses by running the hoarfrost model using the output of a numerical high resolution weather prediction model (Nygaard et al., 2011).

Acknowledgments

The work was supported by IVO Voimansiirto Oy (presently Fingrid), which also provided the transmission loss data. Support by Tekes, Finland and the Nordic Council is acknowledged.

References

Gray, D.M., Male, D.H. (eds.), 1981. Handbook of Snow, Pergamon Press.

Hayashi, Y., Aoki, A., Yuhara, H., 1977. Study of frost formation based on a theoretical model of the frost layer. Heat Transfer-Japanese Res. 6, 79–94.

Kamata, Y., Shishido, M., Iikura, S., Endo, T., 2012. Observation and prediction of trolley wire frosting in the railway field. J. Adhesion Sci. Technol., 26 (4-5), 555-573.

Kandula, M., 2011. Frost growth and densification in laminar flow over flat surfaces. Int. J. Heat Mass Transfer 54, 3719–3731.

Lahti, K., Lahtinen, M., Nousiainen, K., 1997. Transmission line corona losses under hoar frost conditions. IEEE Trans. Power Delivery 12 (2), 928–933.

Mago, P.J., Sherif, S.A., 2005. Frost formation and heat transfer on a cold surface in ice fog. Int. J. Refrigeration 28, 538–546.

Makkonen, L., 1984. A model of ice accretion on wires. J. Climate Appl. Meteorol. 23, 929–939.

Makkonen, L., 1985. Heat transfer and icing of a rough cylinder. Cold Regions Sci. Technol. 10, 105–116.

Makkonen, L., 1992. Analysis of rotating multicylinder data in measuring cloud-droplet size and liquid water content. J. Atmos. Oceanic Technol. 9, 258–263.

Makkonen, L., 2000. Models for the growth of rime, glaze icicles and wet snow on structures. Phil. Trans. R. Soc. Lond. A, 358, 2913–2939.

Makkonen, L., Laakso, T., 2005. Humidity measurements in cold and humid environments. Boundary-Layer Meteorol. 116, 131–147.

Nygaard, B.E.K., Kristjánsson, J.E., Makkonen, L., 2011. Prediction of in-cloud icing conditions at ground level using the WRF model. J. Climate Appl. Meteorol. 50, 2445-2459.

Poots, G., 1996. Ice and Snow Accretion on Structures. Wiley & Sons, pp. 80–83.

Raju, S.P., Sherif, S.A., 1992. Frost formation and heat transfer on circular cylinders in cross flow. Fundamentals of Heat Transfer in Porous Media 193, ASME 1992, 109–121.

Sollerkvist, F.J., Maxwell, A., Rouden, K., Ohnstad,T.M., 2007. Evaluation, verification and operational supervision of corona losses in Sweden. IEEE Trans. Power Delivery, 22 (2), 1210–1217.

Saito, H., Tokura, I., Kishinami, K., Uemura, S., 1984. A study on frost formation. Trans. Japan Soc. Mech. Engr., Ser B 50, 1190–1195 (in Japanese).

Schneider, H.W., 1977. Equation of the growth rate of frost forming on cooled surfaces. Int. J. Heat Mass Transfer Vol. 21 (8), 1019–1024.

Sedlar, J., Hock, R., 2009. Testing longwave radiation parameterizations under clear and overcast skies at Storglaciären, Sweden. The Cryosphere 3, 75–84.

Seki, N., Fukusako, S., Matsuo, K., Uemura, S., 1984. Incipient phenomena of frost formation. Trans. Japan. Soc. Mech. Engr., Ser B 50, 825–831 (in Japanese).

Sparrow, H., Stretton, A.J., 1985. Natural convection from variously oriented cubes and from other bodies of unity aspect ratio. Int. J. Heat Mass Transfer 28, 741–752.

Teisseyre, Y., Farzaneh, M., 1990. On the mechanisms of the ice accretion on H.V. conductors. Cold Regions Sci. Technol. 18, 1–8.

Yonko, J.D., Sepsy, C.F., 1967. An investigation of the thermal conductivity of frost while forming on a flat horizontal plate. ASHRAE Trans. 73, Part II, Paper no. 2043, pp. I1.1–I1.10.

Zhang, X.H., Liu, Z.L., Wang, J.T., Gou, Y.J., Meng, S., Ma, C.F., 2006. Experimental investigation of the influence of electric field on frost layer growth under natural convection condition. Prog. Natural Sci. 16, 410–415.

Östin, R., Andersson, S., 1991. Frost growth parameters in a forced air stream. Int. J. Heat Mass Transfer 34, 1009–1017.